

Adaptive finite element modeling of stationary and propagating cracks in piezoelectric structures

Ł. JAŃSKI, M. KUNA

*Institute of Mechanics and Fluid Dynamics
TU Bergakademie Freiberg
Freiberg, Germany
e-mail: ljanski@poczta.onet.pl*

IN THE PRESENT PAPER, simulation results of stationary and propagating cracks in piezoelectric test specimens are presented. The simulations have been carried out with a self-developed adaptive finite element computer program. Two specimen configurations are investigated, i.e. the compact tension and three-point bending specimens. In the analysis of the propagating crack in the compact tension specimen, the fracture toughness change due to the change of the electric field in the test domain is taken into account. To prove the importance of the fracture toughness anisotropy assumption, crack growth simulations for the three-point bending specimens are reported.

Key words: piezoelectric fracture mechanics, crack propagation simulation, adaptive finite element method.

Copyright © 2011 by IPPT PAN

1. Introduction

PIEZOELECTRIC CERAMICS can be easily found in many modern engineering applications as mechatronics, microsystem technology or smart structures. Due to the intrinsic coupling between mechanical and electrical energy, these materials can serve as sensors, actuators or transducers. This ability is widely used in various technical devices as ultrasonic medical equipment, fuel injection pistons or smart composites with integrated piezoelectric layers. Lead zirconate titanate PZT is the most prominent piezoelectric ceramics which possesses large actuating strain, fast response time and high stiffness. Apart from these great advantages, piezoelectric ceramics have also a considerable disadvantage, that is their inherent brittleness and low fracture toughness. Consequently, piezoelectric ceramics are susceptible to fracture and damage, especially under highly concentrated stresses and electrical fields which may occur in piezoelectric structures due to service loads. Fracture, damage and fatigue emerge as coupled electromechanical phenomena.

To assure sufficient reliability of technical devices, their behaviour with respect to fracture must be evaluated. This concerns both aspects, crack prop-

agation resistance as well as consequences of a crack propagation. In the first case, usually analyses of stationary cracks suffice. In the second case, full crack propagation analyses are necessary. It is important to point out that consideration of materials with internal electromechanical interaction makes necessary investigation of the influence of not only mechanical, but also electrical external loads on fracture.

An actual survey about fracture mechanics concepts for piezoelectric ceramics can be found in [9] and the conference proceedings [10]. One of the most crucial points is subcritical crack growth in multilayer actuators, even when exposed to pure cyclic electric loading [16]. Contrary to this, only a few attempts have been made to simulate crack propagation by numerical methods.

There is quite a lot of scientific literature which describes methods for stationary crack analyses in piezoelectric structures, on the one hand, and presents the results of the analyses on the other hand. In [13], many of the analytical methods are summarized. Numerical algorithms, based on the finite element method, are characterized, e.g. in [5, 3] and [8]. In these algorithms, “handmade” finite element meshes are used. Only in the paper [6], automatically refined meshes are applied to the computation of dielectric and mechanical intensity factors. However, according to the book [17], finite element adaptivity is the state of the art of numerical analyses. Even though there are many works, e.g. [1, 14] and [4] devoted to crack propagation simulations in elastic bodies, there is no literature coping with this subject for piezoelectric structures.

Contrary to the impression that the piezoelectric finite element algorithm is a straightforward extension of the corresponding elastic one, it is important to point out that these two algorithms rely on two different weak formulations belonging to two totally different classes. The piezoelectric weak formulation is a saddle point problem but the classical elastic weak formulation is a minimization problem. This results in systems of linear algebraic equations which also belong to two different classes. In the piezoelectric case, the matrix of coefficients of the system of linear algebraic equations is indefinite. In the classical elastic case, the corresponding matrix is positive definite. Consequently, not all iterative algebraic solvers are reliable in the piezoelectric case.

In the present publication, simulation results of stationary and propagating cracks in piezoelectric specimens are presented. The simulations have been carried out with a self-developed adaptive finite element computer program. In the program, the system of linear algebraic equations is iteratively solved with a variant of the method of conjugate gradients. This variant can be efficiently applied to symmetric but indefinite algebraic systems. The finite element computations take into account monotonic, electromechanical, external loading conditions. Since most of the used fracture mechanical background has been already published in [6], only the untouched aspects are referred in the present work.

Similarly, since the used computational and algorithmic knowhow has been already described in detail in the submitted paper [7], only information required for understanding of the simulation results is recapitulated in the present work.

The structure of the present paper is as follows. In the second section, the governing equations of the piezoelectric boundary value problem are described. The third, fourth and fifth sections are devoted to: the most important features as well as the overall algorithm of the self-developed adaptive finite element computer program, the crack propagation strategy which does not involve remeshing of the whole domain after each crack propagation step and the implemented fracture criterion, respectively. In the sixth section, numerical results obtained for stationary and propagating cracks are presented. Experimental setup described in [15] constitutes the basis for the numerical examples. Thereby, two test configurations are investigated, i.e. the compact tension and the three point bending specimens.

2. Piezoelectric boundary value problem

Let the piezoelectric domain and its boundary be denoted by $\Omega \subset \mathbb{R}^2$ and $\partial\Omega$, respectively. The mechanical Cauchy's equilibrium equations

$$(2.1) \quad \sigma_{\alpha\beta,\beta} + \bar{f}_\alpha = 0 \quad \text{in } \Omega$$

and the Gauss's law of electrostatics

$$(2.2) \quad D_{\alpha,\alpha} = \bar{q} \quad \text{in } \Omega$$

are the fundamental partial differential equations of the analysed electromechanical field problem. In the present publication, Einstein's summation convention is used throughout. Thereby, the subscripts in small Greek letters take values 1 or 2. The comma in a subscript means the partial derivative with respect to the coordinate x_α of the position vector. $\sigma_{\alpha\beta}$, \bar{f}_α , D_α and \bar{q} are the stress tensor, body force vector, electric displacement vector and free electric volume charge density, respectively. To obtain the complete piezoelectric boundary value problem, the differential equations (2.1) and (2.2) are complemented with the natural mechanical

$$(2.3) \quad \sigma_{\alpha\beta} n_\beta = \tilde{T}_\alpha \quad \text{on } \Gamma_T \subset \partial\Omega,$$

natural electrical

$$(2.4) \quad D_\alpha n_\alpha = -\tilde{q} \quad \text{on } \Gamma_q \subset \partial\Omega,$$

essential mechanical

$$(2.5) \quad u_\alpha = \tilde{u}_\alpha \quad \text{on } \Gamma_u \subset \partial\Omega$$

as well as essential electrical

$$(2.6) \quad \varphi = \tilde{\varphi} \quad \text{on} \quad \Gamma_\varphi \subset \partial\Omega$$

boundary conditions. \tilde{T}_α , \tilde{q} , n_α , \tilde{u}_α and $\tilde{\varphi}$ are the traction vector, surface charge density, outer vector normal to the appropriate part of the boundary $\partial\Omega$, prescribed mechanical displacement and prescribed electrical potential, respectively. The mechanical displacement vector u_α is the primary variable of elasticity. The symmetric part of its gradient defines the strain tensor

$$(2.7) \quad \epsilon_{\alpha\beta} = \frac{1}{2} (u_{\alpha,\beta} + u_{\beta,\alpha}).$$

Similarly, the primary variable of electrostatics, the electrical potential φ , allows for the definition of the vector of electrical field

$$(2.8) \quad E_\alpha = -\varphi_{,\alpha}.$$

Piezoelectric materials exhibit the direct and inverse piezoelectric effect. The first of these effects is identified with electric charges generated during deformation. The second effect can be observed when the applied voltage causes deformation. The constitutive equations

$$(2.9) \quad \begin{aligned} \sigma_{\alpha\beta} &= c_{\alpha\beta\gamma\delta} \epsilon_{\gamma\delta} - e_{\omega\alpha\beta} E_\omega, \\ D_\alpha &= e_{\alpha\delta\omega} \epsilon_{\delta\omega} + \kappa_{\alpha\delta} E_\delta, \end{aligned}$$

reflect the above-mentioned effects in the linearized form. $c_{\alpha\beta\gamma\delta}$, $\kappa_{\alpha\beta}$ and $e_{\alpha\beta\delta}$ are the elastic, dielectric and piezoelectric material tensors, respectively.

In the manufacturing process, piezoelectric ceramics are usually poled through the application of a high voltage. After this procedure, the material under consideration is characterized by the poling direction. Existence of this favored direction results in the transversal isotropy. For this special material symmetry type as well as for the plane strain condition, the general constitutive equations (2.9) can be written in the matrix form:

$$(2.10) \quad \begin{bmatrix} \sigma_{11} \\ \sigma_{22} \\ \sigma_{12} \\ D_1 \\ D_2 \end{bmatrix} = \begin{bmatrix} c_{11} & c_{12} & 0 & 0 & -e_{21} \\ c_{12} & c_{22} & 0 & 0 & -e_{22} \\ 0 & 0 & c_{44} & -e_{16} & 0 \\ 0 & 0 & e_{16} & \kappa_{11} & 0 \\ e_{21} & e_{22} & 0 & 0 & \kappa_{22} \end{bmatrix} \begin{bmatrix} \epsilon_{11} \\ \epsilon_{22} \\ 2\epsilon_{12} \\ E_1 \\ E_2 \end{bmatrix}.$$

The relationship (2.10) characterizes a transversely isotropic piezoelectric material with the poling direction parallel to the x_2 -axis.

The partial differential equations (2.1) and (2.2) with the associated natural (2.3) and (2.4) as well as essential (2.5) and (2.6) boundary conditions have been solved with the finite element method.

3. Computer program description

The main feature of the self-developed finite element computer program π CRACK for crack propagation analyses in piezoelectric structures is the application of the finite element adaptivity. This strategy provides the numerical solution whose accuracy, defined with an error estimator, is exactly equal to a certain user-specified error distribution. Thanks to adaptivity, no special finite elements, e.g. singular elements, are necessary to model high gradients of the electromechanical fields in the vicinity of crack tips. This is especially advantageous in case of crack propagation simulations. No extraordinary treatment is necessary for the finite elements in the vicinity of crack tips in each propagation step. Another important feature of the computer program under consideration is the application of a variant of the preconditioned conjugate gradient method for the solution of the system of linear algebraic equations obtained, after the discretisation of the piezoelectric variational formulation. This iterative solution strategy speeds up the solution convergence and minimizes the memory requirements. The two mentioned features are complemented by a special crack propagation algorithm. To realise this propagation, the finite element mesh is modified directly. Consequently, no remeshing of the domain with a crack after each crack propagation step is necessary. The algorithm is simple and can be easily coupled with the h-adaptivity. To compute the dielectric and mechanical intensity factors, the interaction integral technique is applied. These intensity factors are used in the implemented fracture criterion of the maximum modified hoop stress intensity factor. The criterion takes into account the anisotropy of the fracture toughness of piezoelectric ceramics, makes possible, to some extent, prediction of the electric loading influence on fracture and is applicable to non-self-similar crack growth, i.e. for mixed mode fracture.

In Fig. 1, a flowchart of the algorithm is presented which is used in the computer program π CRACK. In the module π SOLVE, the piezoelectric boundary value problem is solved with the adaptive finite element method. The finite element solution is used in the module π FRPAR for the computation of the dielectric and mechanical intensity factors. On the basis of the intensity factors, in the module π FRCRIT, the decision is undertaken if the crack propagates or not. In the case of crack growth, the fracture direction is computed. This direction is used for the finite element mesh adjustment in the module π FRGROW. After the mesh modification, a new finite element solution is searched in the module π SOLVE.

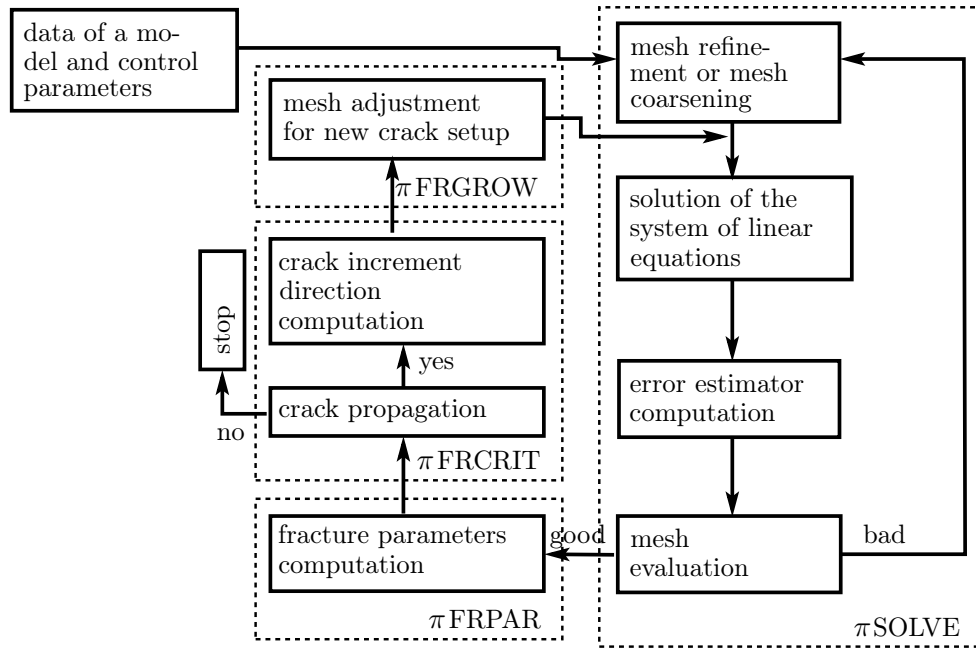


FIG. 1. Flowchart of the algorithm used in the computer program π CRACK.

In Fig. 2, a scheme of a propagating crack and characteristic angles are presented. The tangent line is defined in the crack tip as the limit of all tangent lines to the existing crack and approaching the crack tip. (r, θ) is a polar coor-

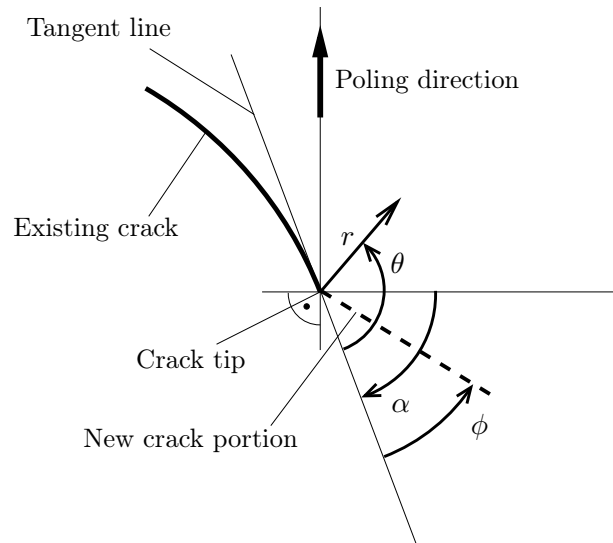


FIG. 2. Propagating crack scheme.

dinate system with the origin at the crack tip. The ray defined by $\theta = 0$ lies on the tangent line and points opposite to the existing crack direction. The angle α describes the orientation of the ray $\theta = 0$ with respect to the poling direction of the material. The angle ϕ represents the propagation direction of the new crack portion with respect to the existing one.

4. Crack propagation algorithm

Because of the crack propagation, additional crack surfaces are created both of length Δa . This causes a corresponding change of the domain boundary and consequently, of the piezoelectric boundary value problem. The so far geometrically continuous regions of the domain are now splitted by the new crack segment. Since classical finite elements are continuous regions, the splitting must be realized along finite element edges. On the other hand, the direction and length of a new crack segment are usually determined by physical factors. It means, the direction and length have to be chosen independently of the finite element mesh. Consequently, in the general case, generation of new nodes, edges and elements is necessary to model crack propagation on the finite element level. In the module π FRGROW of the computer program, they are generated by the element splitting algorithm, which is graphically presented in Fig. 3. Thereby, S_1 corresponds to the tip of the initial crack and S_2 to the tip of the crack after propagation. ϕ is the propagation angle already introduced in Fig. 2. Δa is the

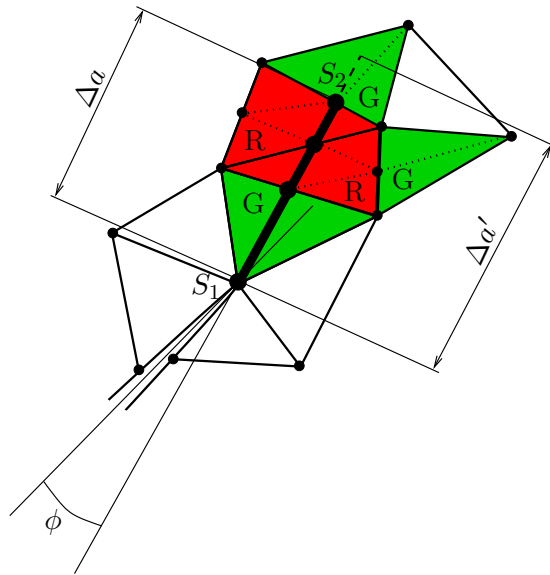


FIG. 3. Element splitting algorithm.

propagation length. The mentioned algorithm works as follows. At first, intersection points are searched between a test segment of length $\Delta a' > \Delta a$ and all cut finite element edges. In those intersection points, new finite element nodes are pairwise (except the new crack tip S_2 where only one node is introduced) defined. The new nodes are connected in such a way that pairs of finite element edges are created. In the element splitting process, two characteristic variants can be distinguished. In the first variant (green), only one of the edges of a certain finite element is cut by the test segment. In the second variant (red), exactly two of the edges of a certain finite element are cut by the test segment. The corresponding description G (green) and R (red) is used in Fig. 3. The green splitting of an initial finite element results in two new elements, and the red one in four new elements.

5. Fracture criterion

Considering the choice of appropriate fracture criteria for piezoelectric materials, it is important to state, already at the early beginning, that suitable fracture criteria for piezoelectric materials are still being searched for. There are of course several classical possibilities, like e.g. the criterion of the maximal energy release rate. Application of this criterion to piezoelectric problems leads, however, to the conclusion that the electric field always impedes crack growth regardless of the direction of the electric field applied [11]. This conclusion is not consistent with experimental observations. On the other hand, the maximum mechanical energy release rate criterion, proposed in [11], is doubtful due to different treatment of mechanical and electrical energies. No profound explanation exists, why the electrical energy part in the total energy release rate may be neglected. The criterion of the maximum modified hoop stress intensity factor, presented in [18], fails e.g. in the case of pure electrical loading. For this loading, no crack propagation is predicted with the fracture criterion under consideration, whereas experimental findings are opposite. In order to test the criterion of the maximum modified hoop stress intensity factor more carefully, it has been implemented in the finite element computer program π CRACK.

Measurements of the fracture toughness of polarized piezoceramics show that the toughness K_c^{\parallel} in direction parallel to the poling direction is higher than the toughness K_c^{\perp} in direction perpendicular to the poling direction [12]. The reported ratio $K_c^{\parallel}/K_c^{\perp}$ ranges from 1.15 to 2.36 for different piezoceramics. To obtain the fracture toughness in any direction, the interpolation formula

$$(5.1) \quad K_c(\theta) = K_c^{\perp} \cos^2(\theta + \alpha) + K_c^{\parallel} \sin^2(\theta + \alpha)$$

can be used [18]. The hoop stress intensity factor is defined as

$$(5.2) \quad K_{\theta\theta}(\theta) = \lim_{r \rightarrow 0} \sqrt{2\pi r} \sigma_{\theta\theta}(\theta)$$

and the modified hoop stress intensity factor as

$$(5.3) \quad K^*(\theta) = K_{\theta\theta}(\theta) / K_c(\theta).$$

In Eq. (5.2), $\sigma_{\theta\theta}(\theta)$ represents the hoop stress. Using the criterion of the modified hoop stress intensity factor, the crack growth direction θ_{\max} is predicted which guarantees maximal modified hoop stress intensity factor. The crack propagates in this direction if the condition

$$(5.4) \quad K_{\theta\theta}(\theta_{\max}) \geq K_c(\theta_{\max})$$

is satisfied. Since the developed finite element computer program should be applicable to general crack propagation problems, a scan over all angles around the actual crack tip is realized to predict the crack growth direction θ_{\max} .

6. Numerical examples

The computer program π CRACK has been used to analyze stationary cracks in two test configurations, i.e. the compact tension and the three-point bending specimens. The geometry of the specimens, boundary conditions and the used material parameters, presented in Table 1, correspond to the experimental setup described in [15]. The choice of the supercritical electromechanical loading has also enabled crack propagation simulations. The detailed geometry of the specimens is shown in Figs. 4 and 5, whereby millimeters are used as units of length. The cracks are assumed to be electrically impermeable. This leads to the following electrical boundary condition on crack faces

$$(6.1) \quad D_n^+ = D_n^- = 0.$$

The normal component of the electric displacement vector to the crack faces is continuous across the crack faces and equals zero. The superscripts + and – denote the upper and lower crack faces. This impermeability assumption corre-

Table 1. Material parameters of the PZT4 piezoelectric ceramic.

c_{11} (N/m ²)	c_{22} (N/m ²)	c_{13} (N/m ²)	c_{12} (N/m ²)	c_{44} (N/m ²)
$1.39 \cdot 10^{11}$	$1.13 \cdot 10^{11}$	$7.78 \cdot 10^{10}$	$7.43 \cdot 10^{10}$	$2.56 \cdot 10^{10}$
e_{16} (C/m ²)	e_{21} (C/m ²)	e_{22} (C/m ²)	κ_{11} (C ² /N m ²)	κ_{22} (C ² /N m ²)
13.44	–6.98	13.84	$6.00 \cdot 10^{-9}$	$5.47 \cdot 10^{-9}$

sponds well with the high dielectric constant of the medium in crack gaps, which has been used in the experiments described in [15]. In all numerical examples taking into account anisotropy of the fracture toughness of piezoelectric ceramics, the ratio $K_c^{\parallel}/K_c^{\perp} = 2$ is chosen.

6.1. Compact tension specimen

In Fig. 4, the model of the analyzed compact tension specimen is presented. The applied external voltage U generates an electric field with mean magnitude E_2 . The magnitudes of the force F and the electric field E_2 depend on the particular test being carried out and are, in each case, specified later on in the text. The stiffness of the thin, flexible, metallic electrodes can be neglected compared with that of the piezoelectric ceramic. In Fig. 5, the initial finite element

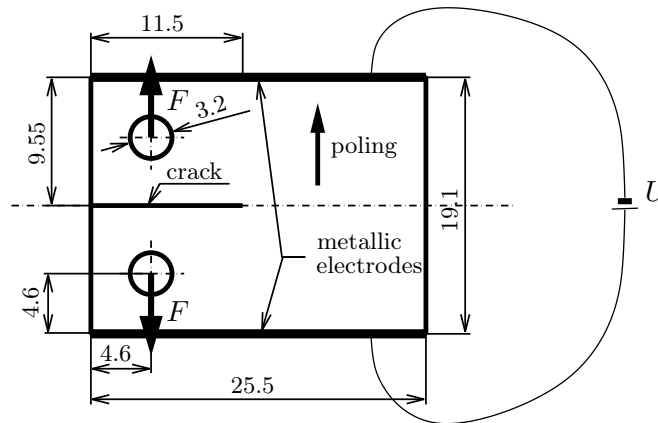


FIG. 4. Compact tension specimen model.

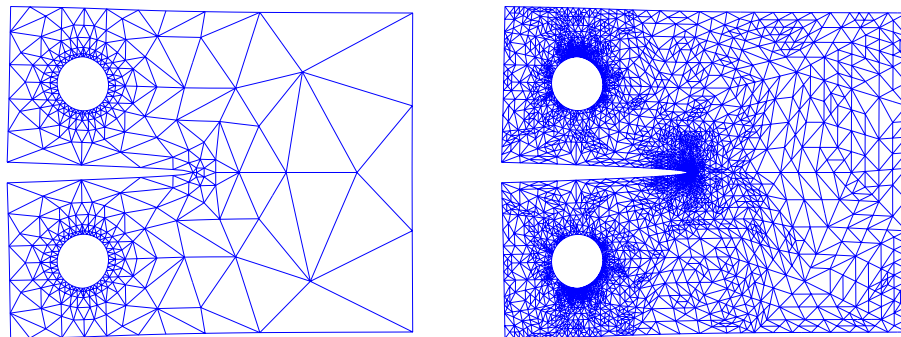


FIG. 5. Finite element meshes: initial (left) and in the twelfth refinement step (right).

triangulation as well as the finite element mesh, obtained in the twelfth refinement step of the implemented adaptive algorithm, are presented. In Fig. 6, values of the computed mechanical intensity factors K_I , K_{II} and the dielectric intensity factor K_{IV} are plotted as a function of the refinement step. Fast stabilization of the intensity factors can be observed after a few refinements. Since the crack in the compact tension specimen opens only in modes I and IV , the computed intensity factor K_{II} is equal to zero as expected. In [15], the experimentally obtained critical values of the force F are published which correspond to the initiation of crack propagation. These forces are different for different electric fields E_2 in each of the six performed tests. Let us denote any electromechanical loading necessary for the initiation of crack growth as (F_c, E_{2c}) .

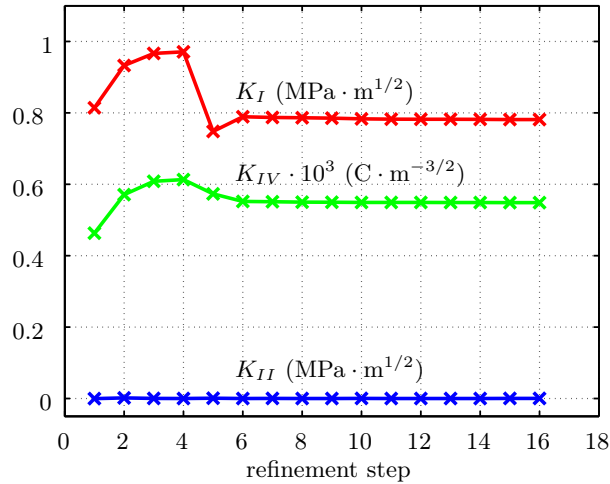


Fig. 6. Adaptive convergence of intensity factors for $F = 85$ N and $E_2 = 2.62$ kV/cm.

In Table 2, these electromechanical loadings, the corresponding values of the critical intensity factors and energy release rates are presented. K_{Ic} and

Table 2. Critical load and fracture parameters.

No.	F_c (N)	E_{2c} (kV/cm)	K_{Ic} (MPa · m ^{-1/2})	K_{IVc} (C · m ^{-3/2})	G_c (N/m)	G_c^M (N/m)
1	66.0	10.47	0.593	1.587e-3	-86.183	13.52
2	72.0	5.24	0.652	0.879e-3	-17.379	10.07
3	79.0	2.62	0.726	0.535e-3	0.689	8.916
4	97.0	0.0	0.877	0.212e-3	8.851	8.757
5	108.0	-2.62	0.976	-0.124e-3	5.352	7.268
6	126.0	-5.24	1.165	-0.434e-3	-7.544	6.274

K_{IVc} have been computed by means of the adaptive finite element program π CRACK. G^M is the mechanical part, introduced in [11], of the energy release rate G . G_c and G_c^M have been obtained using K_{Ic} , $K_{IIc} = 0$ and K_{IVc} , as well as Irwin's matrix and Irwin's formula, both cited in [6].

Table 3. Comparison of energy release rates with values from the literature.

No.	G_c (N/m)	\bar{G}_c [2] (N/m)	$ \Delta G_c /\bar{G}_c$ (%)	G_c^M (N/m)	\bar{G}_c^M [2] (N/m)	$ \Delta G_c^M /\bar{G}_c^M$ (%)
1	-86.183	-85.91	0.32	13.52	13.26	1.96
2	-17.379	-17.38	0	10.07	10.01	0.6
3	0.689	0.44	56.59	8.916	8.66	2.96
4	8.851	8.81	0.46	8.757	8.64	1.35
5	5.352	4.86	10.12	7.268	6.61	9.95
6	-7.544	-8.77	13.97	6.274	4.93	27.26

In Table 3, the values of G_c and G_c^M from Table 2 are compared with the values reported in [2]. Fluctuation of the relative error can be observed. However, most of the corresponding results are in agreement. In Fig. 7, the dependence of K_{Ic} , G_c and G_c^M on K_{IVc} is plotted on the basis of Table 2. All three functions are not constant. Assuming that the fracture toughness K_c^\perp is equal to the intensity factor K_{Ic} , it can be easily recognized that the force $F = 85$ N, lying slightly over the critical force in Table 2, and electric field $E_2 = 2.62$ kV/cm lead to satisfaction of the crack propagation condition (5.4). Consequently, the

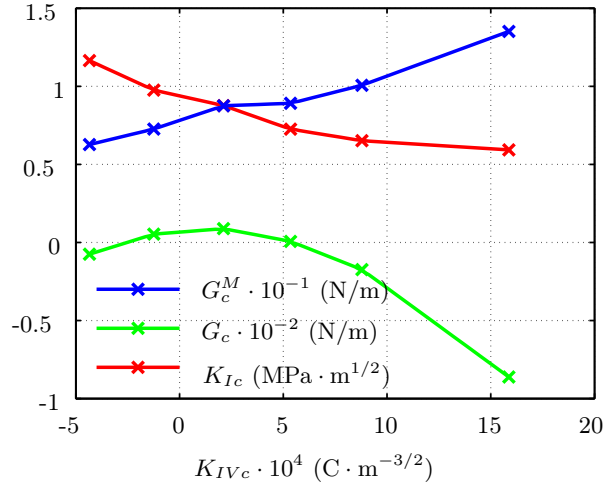


FIG. 7. Dependence of energy release rates G_c , G_c^M and mechanical intensity factor K_{Ic} on dielectric intensity factor K_{IVc} .

crack initiates and an accelerated propagation takes place under constant force loading. By means of the program π CRACK, a quasi-static simulation without inertia effects was carried out.

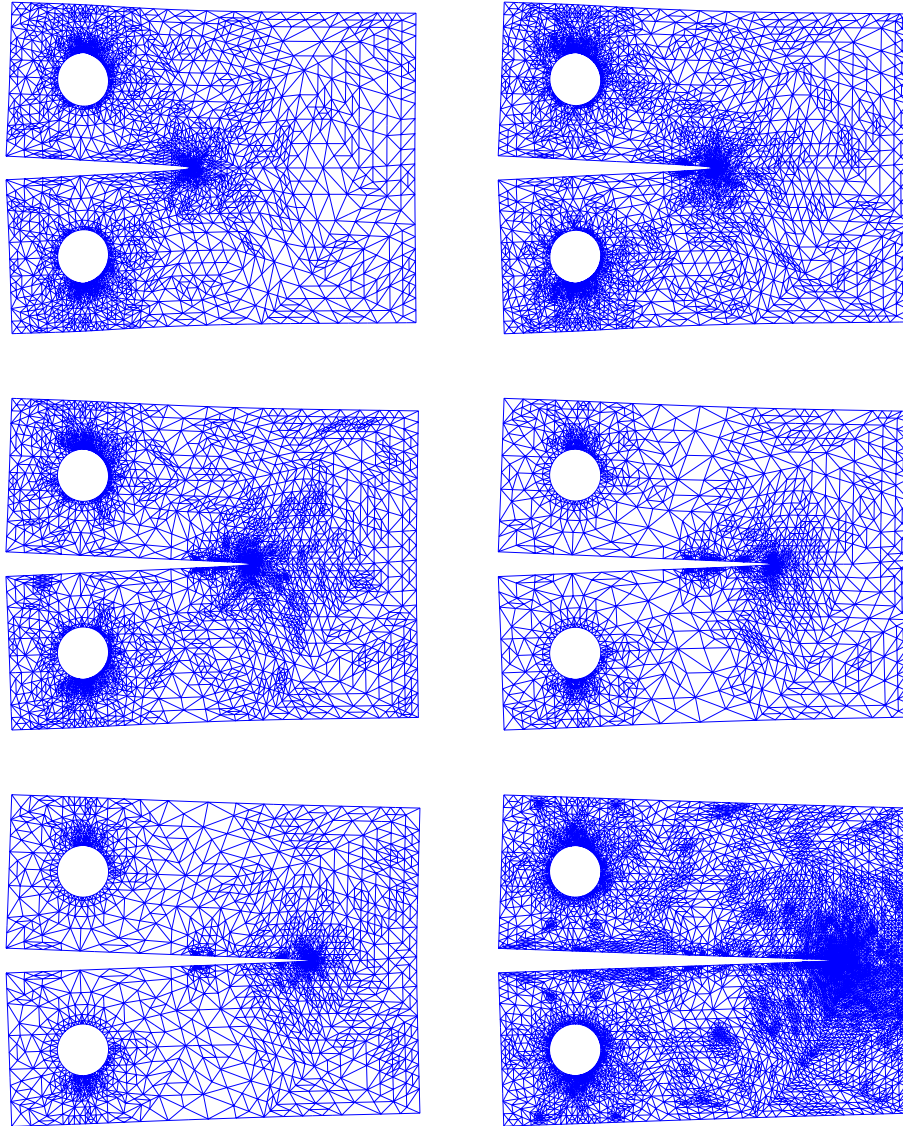


FIG. 8. Finite element meshes generated just before one of the six crack propagation steps.

In Fig. 8, finite element meshes are shown which have been automatically generated during the simulation of crack growth. Thereby, only those meshes are chosen which have been generated just before one of the crack propagation steps.

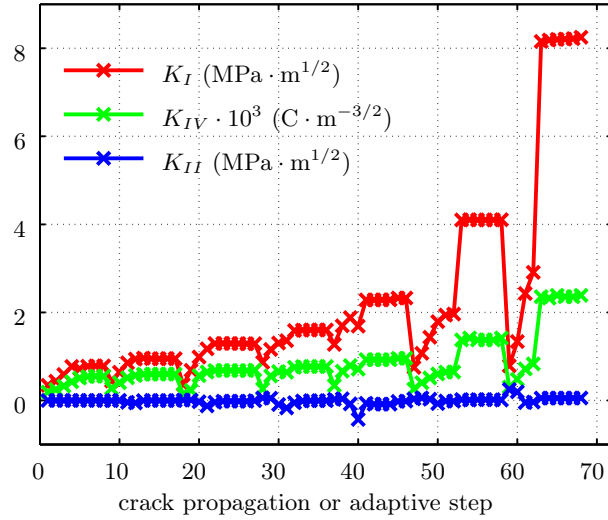


FIG. 9. Intensity factors for crack propagation and adaptive steps for $F = 85$ N and $E_2 = 2.62$ kV/cm.

In Fig. 9, mechanical and dielectric intensity factors are plotted as a function of crack propagation or adaptive step. Six crack propagation steps are performed, each followed by adaptive steps until stabilization of the intensity factors. The stabilized intensity factors K_I and K_{IV} as well as the intensity factor K_{Ic} are plotted in Fig. 10. Thereby, the dependence of K_{Ic} on K_{IVc}

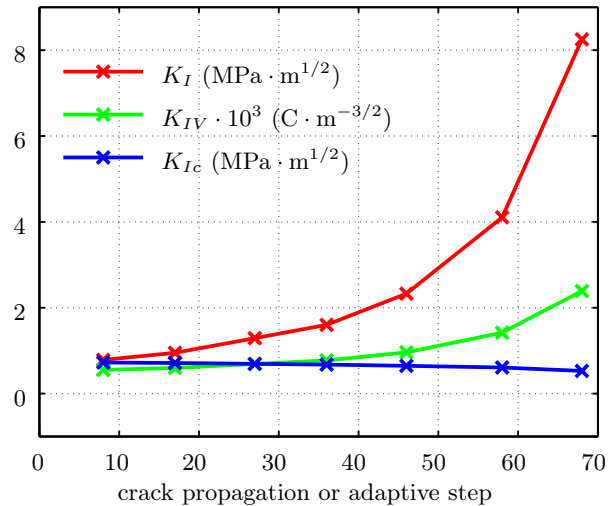


FIG. 10. Converged intensity factors K_I and K_{IV} as well as the corresponding fracture toughness K_{Ic} for propagating crack under $F = 85$ N, $E_2 = 2.62$ kV/cm.

has been taken into account. Since the experimental data used in this paper are available only for discrete points, linear interpolation and extrapolation had to be applied to obtain values of K_{Ic} for the computed values of K_{IV} . Analyzing the diagram in Fig. 10, one can easily conclude that the change of K_{Ic} due to the electric field can be neglected for the experiment under consideration.

6.2. Three-point bending specimen

In Fig. 11, the model of the analyzed three-point bending specimen is presented. The voltage U generates the electric field $E_2 = 5$ kV/cm. The specimen is loaded with the force $F = 165$ N. In [15], different specimens with three locations of the initial crack with respect to the axis of symmetry of the specimen have been experimentally investigated. Since the location on the axis of symmetry leads to qualitatively similar results to the ones of the compact tension specimen, only the two remaining asymmetric initial crack configurations are analyzed in this publication. The complete set of results is presented for the specimen with the 4 mm off-center initial crack. For the specimen with the 2 mm off-center initial crack, only the computed crack paths for the anisotropic and isotropic fracture toughnesses are shown. Once again, the stiffness of the thin, flexible, metallic electrodes can be neglected compared with that of the piezoelectric ceramic.

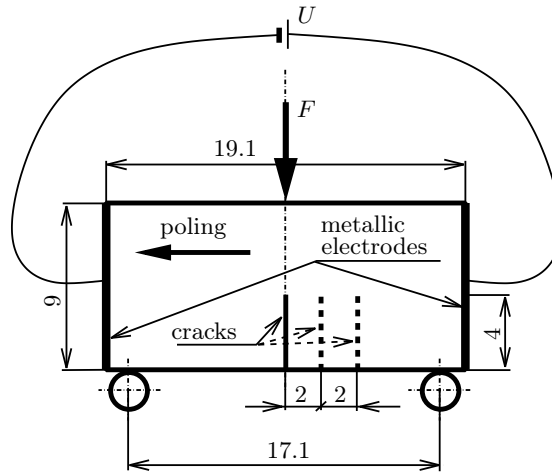


FIG. 11. Three point bending specimen model.

In Fig. 12, the initial finite element triangulation as well as the finite element mesh, obtained in the twelfth refinement step of the implemented adaptive algorithm are depicted. In Fig. 13, values of the computed intensity factors are plot-

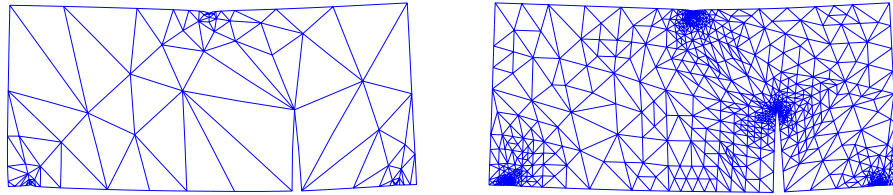


FIG. 12. Finite element meshes: initial (left) and after twelve refinement steps (right).

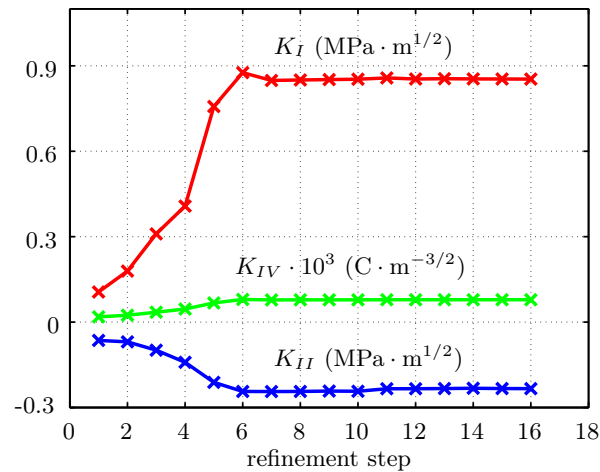


FIG. 13. Adaptive convergence of intensity factors.

ted as a function of the refinement step. Fast stabilization of the intensity factors can be observed. Assuming that the fracture toughness $K_c^\perp = 0.63 \text{ MPa} \cdot \text{m}^{-1/2}$ and assuming that the fracture toughness distribution $K_c(\theta)$ do not depend on the electric field but is only expressed with Eq. (5.1), the crack propagation condition (5.4) is satisfied. Consequently, crack propagation analysis is possible.

In Fig. 14, finite element meshes are depicted which have been automatically generated during the simulation of crack growth. Thereby, only those meshes are chosen which have been generated just before one of the crack propagation steps. In Fig. 15, intensity factors are plotted as a function of crack propagation or adaptive steps. Six crack propagation steps each are followed by adaptive steps until stabilization of the intensity factors. As a consequence of the anisotropic fracture toughness, the mechanical intensity factor K_{II} is not equal to zero along the whole crack path. If one assumes the isotropic fracture toughness, the crack

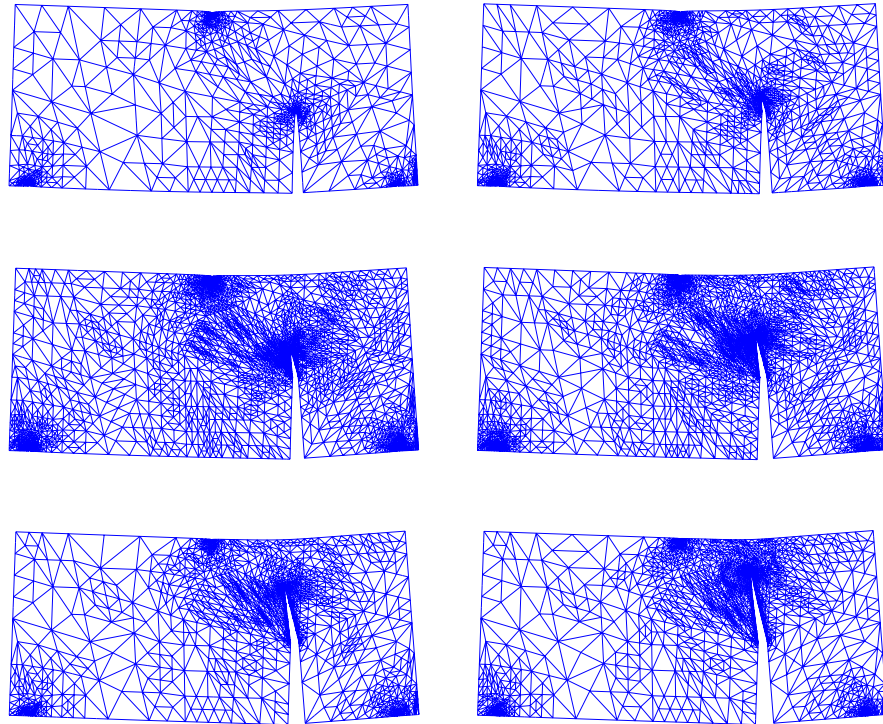


FIG. 14. Finite element meshes generated just before one of the six crack propagation steps.

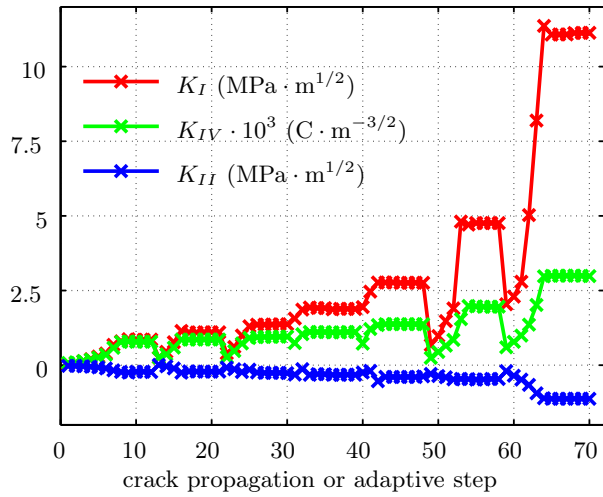


FIG. 15. Intensity factors for crack propagation and adaptive steps (anisotropic fracture toughness).

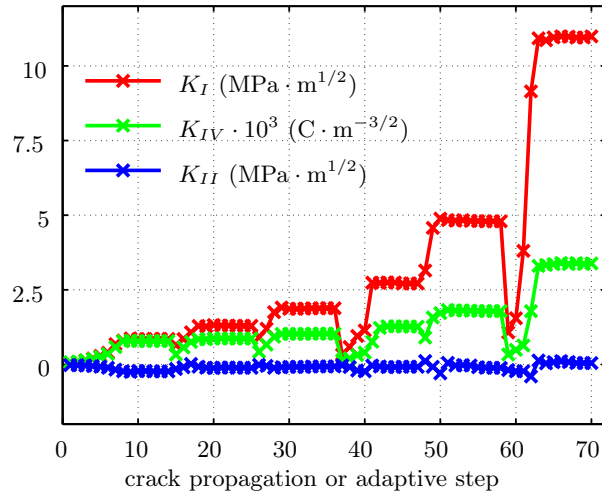


FIG. 16. Intensity factors for crack propagation and adaptive steps (isotropic fracture toughness).

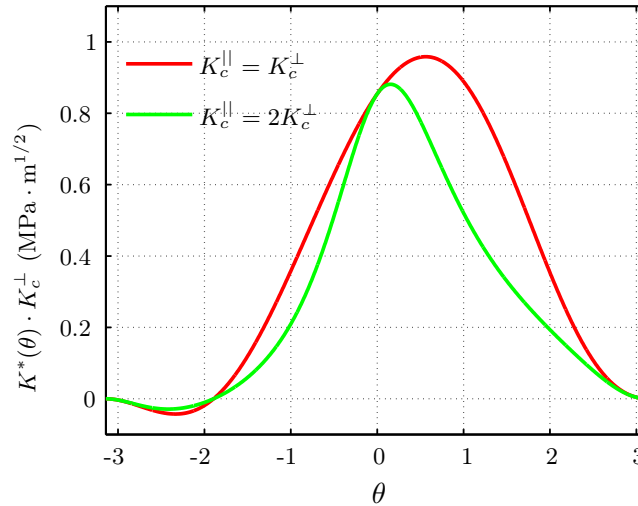


FIG. 17. Modified hoop stress intensity factor around the crack tip before the first propagation step.

propagates along the path, where the mechanical intensity factor K_{II} is equal to zero. This fact can be observed in Fig. 16. To analyze the crack propagation angle in the first crack propagation step for both the isotropic and anisotropic fracture toughnesses, the modified hoop stress intensity factor is shown in Fig. 17 as a function of the angle θ . The maxima of the functions for the isotropic and anisotropic case lie at 25° and 7° , respectively. The result for the anisotropic case

is much closer to the experimentally obtained value in [15], i.e. 5° . Consequently, the anisotropy of the fracture toughness is an important factor influencing the crack propagation path. In Fig. 18, crack paths are presented for the anisotropic and isotropic fracture toughnesses, as well as 4 mm and 2 mm off-center initial cracks.

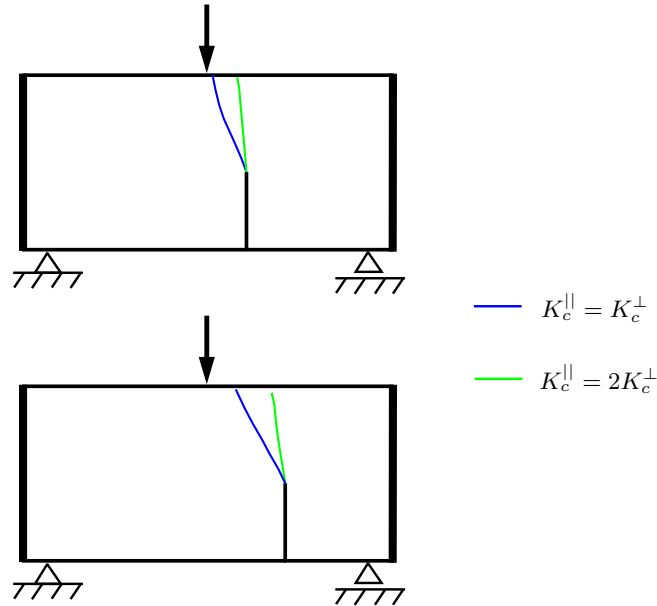


FIG. 18. Crack paths for anisotropic and isotropic fracture toughnesses as well as 4 mm (lower figure) and 2 mm (upper figure) off-center initial cracks.

To give the Reader an insight into the efficiency of the finite element algorithm used in this publication, the following statements can be formulated. The computations of stationary crack problems take several minutes on a middle class PC with one processor. The simulations of propagating crack problems can take up to several hours on the same type of computers.

7. Conclusions

The self-developed adaptive finite element computer program π CRACK can be efficiently used for simulations of both the stationary and propagating cracks in two-dimensional piezoelectric components. The mechanical and dielectric intensity factors, the mechanical and total energy release rates as well as crack paths can be computed with high accuracy. The analysis of the propagating crack in the compact tension specimen takes into account the fracture toughness change due to the change of the electric field in the domain. The computations

show, however, that the increase of the mechanical intensity factor K_I during crack growth is much higher than the change of the fracture toughness. Consequently, for the experiment under consideration, the influence of the electric field on the mentioned toughness can be neglected during crack propagation. In the analysis of the propagating crack in the three-point bending specimen, the importance of the fracture toughness anisotropy assumption is tested. Comparison of the computed and experimentally obtained crack propagation angles in the first crack growth step proves this assumption to be essential. On the other hand, a nonnegligible deviation of the computed and experimentally obtained crack paths can be observed for succeeding crack growth steps. One of the potential reasons may be associated with inertia effects during dynamic crack propagation in the experiments. This fact should be taken into account more carefully in the future developments.

References

1. A.M. ALSHOAIBI, M.S.A. HADI, A.K. ARIFFIN, *An adaptive finite element procedure for crack propagation analysis*, Journal of Zhejiang University Science A, **8**, 228–236, 2007.
2. H. BALKE, J. DRESCHER, G. KEMMER, *Investigation of the mechanical strain energy release rate with respect to a fracture criterion for piezoelectric ceramics*, International Journal of Fracture, **89**, L59–L64, 1998.
3. L. BANKS-SILLS, Y. MOTOLA, L. SHEMESH, *The m -integral for calculating intensity factors of an impermeable crack in a piezoelectric material.*, Engineering Fracture Mechanics, **75**, 901–925, 2008.
4. T. BELYTSCHKO, T. BLACK, *Elastic crack growth in finite elements with minimal remeshing*, International Journal for Numerical Methods in Engineering, **45**, 601–620, 1999.
5. M. ENDERLEIN, A. RICOEUR, M. KUNA, *Finite element techniques for dynamic crack analysis*, International Journal of Fracture, **134**, 191–208, 2005.
6. Ł. JAŃSKI, M. SCHERZER, P. STEINHORST, M. KUNA, *Adaptive finite element computation of dielectric and mechanical intensity factors in piezoelectrics with impermeable cracks*, International Journal for Numerical Methods in Engineering, **81**, 1492–1513, 2010.
7. Ł. JAŃSKI, P. STEINHORST, A. MEYER, *Adaptive finite element computer program with preconditioned iterative algebraic solver for crack propagation simulations in piezoelectric structures*, Computational Mechanics, submitted.
8. M. KUNA, *Finite element analyses of cracks in piezoelectric structures: a survey*, Archives of Applied Mechanics, **76**, 725–745, 2006.
9. M. KUNA, *Fracture mechanics of piezoelectric materials - where are we right now?*, Engineering Fracture Mechanics, **77**, 309–326, 2010.
10. M. KUNA, A. RICOEUR [Eds.], *Proceedings of the IUTAM Symposium on Multiscale Fatigue, Damage and Fracture in Smart Materials*, Springer, Heidelberg, 2011.
11. S.B. PARK, C.T. SUN, *Effect of electric field on fracture of piezoelectric ceramics*, International Journal of Fracture, **70**, 203–216, 1995.

-
12. G.G. PISARENKO, V.M. CHUSHKO, S.P. KOVALEV, *Anisotropy of fracture toughness of piezoelectric ceramics*, Journal of the American Ceramic Society, **68**, 259–265, 1985.
 13. Q.-H. QIN, *Fracture Mechanics of Piezoelectric Materials*, WIT Press, Southampton, 2001.
 14. F. RABOLD, A. MEYER, M. SCHERZER, *Efficient finite element simulation of crack propagation using adaptive iterative solvers*, Communications in Numerical Methods in Engineering, **22**, 93–108, 2006.
 15. C.T. SUN, S.B. PARK, *Fracture criteria for piezoelectric ceramics*, Journal of the American Ceramic Society, **78**, 1475–1480, 1995.
 16. K. UCHINO, *Materials issues in design and performance of piezoelectric actuators: An overview*, Acta Materialia, **48**, 3745–3753, 1998.
 17. P. WRIGGERS, *Nichtlineare Finite-Elemente-Methoden*, Springer-Verlag, Berlin, 2001.
 18. X.-L. XU, R.K.N.D. RAJAPAKSE, *A theoretical study of branched cracks in piezoelectrics*, Acta Materialia, **48**, 1865–1882, 2000.

Received March 18, 2011; revised version September 22, 2011.
